Supplementary Material for

"Multi-dimensional Multiplexing Holography Based on Optical Orbital Angular Momentum Lattice Multiplexing"

Tian Xia[1], Zhenwei Xie[1,*] and Xiaocong Yuan[1,2,*]

[1]*Nanophotonics Research Centre, Institute of Microscale Optoelectronics & State Key Laboratory of Radio Frequency Heterogeneous Integration, Shenzhen University, Shenzhen 518060, China*

[2]*Research Institute of Intelligent Sensing, Research Center for Humanoid Sensing, Zhejiang Lab, Hangzhou 311100, China*

*E-mail: ayst31415926@szu.edu.cn; xcyuan@szu.edu.cn

Supplementary Note1: The orthogonality of VL beams

The orthogonality of the two VL beams can be easily demonstrated by investigating the inner product of the two VL beams. The inner product of the two VL beams with (l_1, α_1, β_1) and (l_2, α_2, β_2) is given as follows:

$$I = \int_0^{2\pi} \int_0^R \exp[i\varphi_{l_1,\alpha_1,\beta_1}] \left\{ \exp[i\varphi_{l_2,\alpha_2,\beta_2}] \right\}^* r dr d\theta \tag{S1}$$

where symbol '*' indicates conjugation.

For the orthogonality of the two VL beams with different parameter l, Eq. (S1) can be written as:

$$I = \int_0^{2\pi} \int_0^R \exp[i\varphi_{l_1}] \left\{ \exp[i\varphi_{l_2}] \right\}^* r dr d\theta \tag{S2}$$

The above inner product is shown in Fig. S1(a). It can be seen that the two VL beams can be considered as orthogonal when the difference between the values of l_1 and l_2 is larger than 1.

For the orthogonality of the two VL beams with different parameter α, Eq. (S1) can be written as:

$$I = \int_0^{2\pi} \int_0^R \exp[i\varphi_{\alpha_1}] \left\{ \exp[i\varphi_{\alpha_2}] \right\}^* r dr d\theta \tag{S3}$$

The above inner product is shown in Fig. S1(b). It can be seen that the two VL beams can be considered as quasi-orthogonal when the difference between the values of α_1 and α_2 is larger than 0.1.

For the orthogonality of the two VL beams with different parameter β, Eq. (S1) can be written as:

$$I = \int_0^{2\pi} \int_0^R \exp[i\varphi_{\beta_1}] \left\{ \exp[i\varphi_{\beta_2}] \right\}^* r dr d\theta \tag{S4}$$

The inner product mentioned above is shown in Fig. S1(c). It is evident that the two VL beams can be considered orthogonal when there is a difference of 0.001 between the values of β_1 and β_2.

Therefore, in certain situations, both the parameters l, α, and β can be regarded as orthogonal parameters. The vortex lattice exhibits n-fold rotational symmetry, where α ranges from 0 to $2\pi/n$. The parameter β is constrained to be less than $\pi/2$. The difference between adjacent β values ranges from 0 to 0.003 to ensure that holographic images overlap without being identified. The parameter l can take any value. Once these specific conditions are met, l, α, and β become independent and orthogonal to each other. A larger l corresponds to a larger size of the OAM beam, without any restrictions on the choice of β. However, excessively large or small l values can impact the system aperture, while similarly, excessively large or small β values can affect the system's field-of-view.
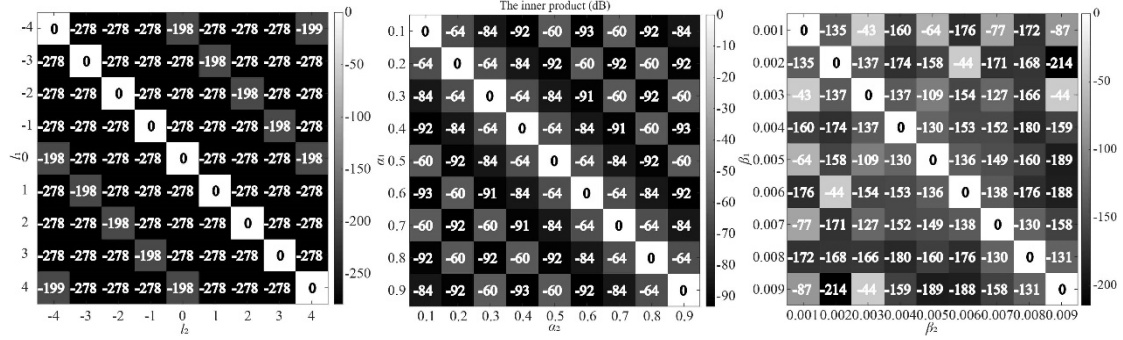

Fig. S1 (a) The numerical simulation of the inner product between the two VL beams with (l_1, 0.1, 0.001) and (l_2, 0.1, 0.001). (b) The numerical simulation of the inner product between the two VL beams with (1, α_1, 0.001) and (1, α_2, 0.001). (c) The numerical simulation of the inner product between the two VL beams with (1, 0.1, β_1) and (1, 0.1, β_2).

Supplementary Note2: The misalignment of incident VL beams

We have provided a thorough analysis to examine the impact of introducing an additional SLM, taking misalignment into consideration. In this scenario, we conducted an investigation on the effects of horizontal and vertical deviations between the generated VL beam and the hologram on the reconstructed image. To assess the disparity between the restored image and the ideal image, we utilized the mean squared error (MSE) as a quantitative measure. The MSE can be computed using the formula: $MSE = \dfrac{1}{M \times N}\sum\limits_{i=1}^{M}\sum\limits_{j=1}^{N}\left(f^{'}(i,j) - f(i,j)\right)^2$, where $f^{'}(i,j)$ and $f(i,j)$ represent corresponding pixel values in the restored image and ideal image respectively, and M and N are the number of the horizontal and vertical pixels respectively. This metric offers insight into the fidelity

of the reconstructed image compared to the desired result. Figure S2 illustrates the correlation between the MSE and both horizontal and vertical deviations. The incident vortex carries a topological charge of 5. Notably, decreasing the absolute value of the horizontal or vertical deviation results in a corresponding decrease in the MSE. This trend implies that smaller deviations yield lower MSE values, indicating a closer match between the restored and ideal images. Specifically, an MSE less than 0.45×10^{-4} allows for obtaining the reconstructed image through the 2D Dirac comb filter. At this point, the horizontal or vertical deviation tolerance is about 2.5 mm, which is more than sufficient for an optical system with an adjustment resolution of tens of micrometers. The simulation results demonstrate the robustness of the proposed concept against misalignments between the two SLMs.
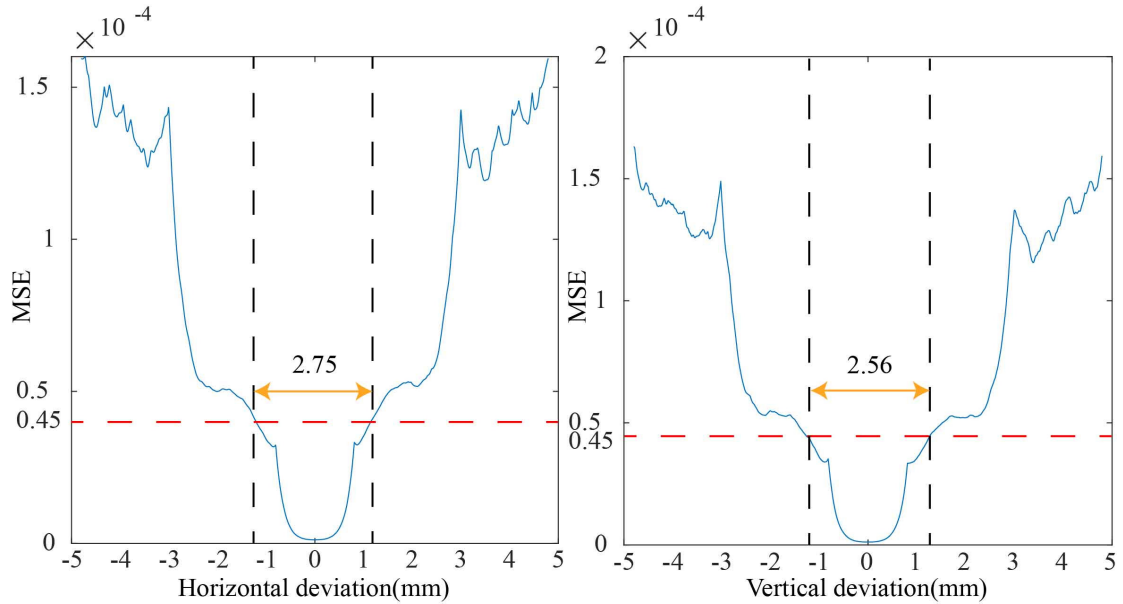

Fig. S2 The plot of the (a) horizontal or (b) vertical deviation and MSE.

Supplementary Note3: The l-α-encrypted OAML-multiplexed holography

The l-α-encrypted OAML-multiplexed holography is shown in Fig. S3. Two different topological charges ($l=1$ and 31) and two different constants α ($\alpha=0.2\pi/2$ and $0.7\pi/2$) are used to encode the four images with the letters "A", "B", "C" and "D". One l-α-encrypted OAML-multiplexed hologram can be obtained by superimposing the four OAM selective holograms generated from the OAM-preserved holograms and four OAML phase modes with ($l=1$, $\alpha=0.2\pi/2$, $\beta=0.001$), ($l=1$, $\alpha=0.7\pi/2$, $\beta=0.001$), ($l=31$, $\alpha=0.2\pi/2$, $\beta=0.001$) and ($l=31$, $\alpha=0.7\pi/2$, $\beta=0.001$). Here l and α together determine the encrypted and decrypted images. The four images can be reconstructed when the multiplexed

hologram is illuminated by different OAML beams with (l=-1, {α}*=-0.2π/2, {β}*=-0.001), (l=-1, {α}*=-0.7π/2, {β}*=-0.001), (l=-31, {α}*=-0.2π/2, {β}*=-0.001) and (l=-31, {α}*=-0.7π/2, {β}*=-0.001), respectively, as shown in Figs. S3(b)–S3(e). Figures S3(f)-S3(i) illustrate the capture intensity distributions of the aforementioned VL beams, respectively. Upon illumination of the multiplexed OAML-preserved hologram by a planar beam, four images manifest simultaneously, appearing indistinguishable from each other, as depicted in Fig. S3(j).
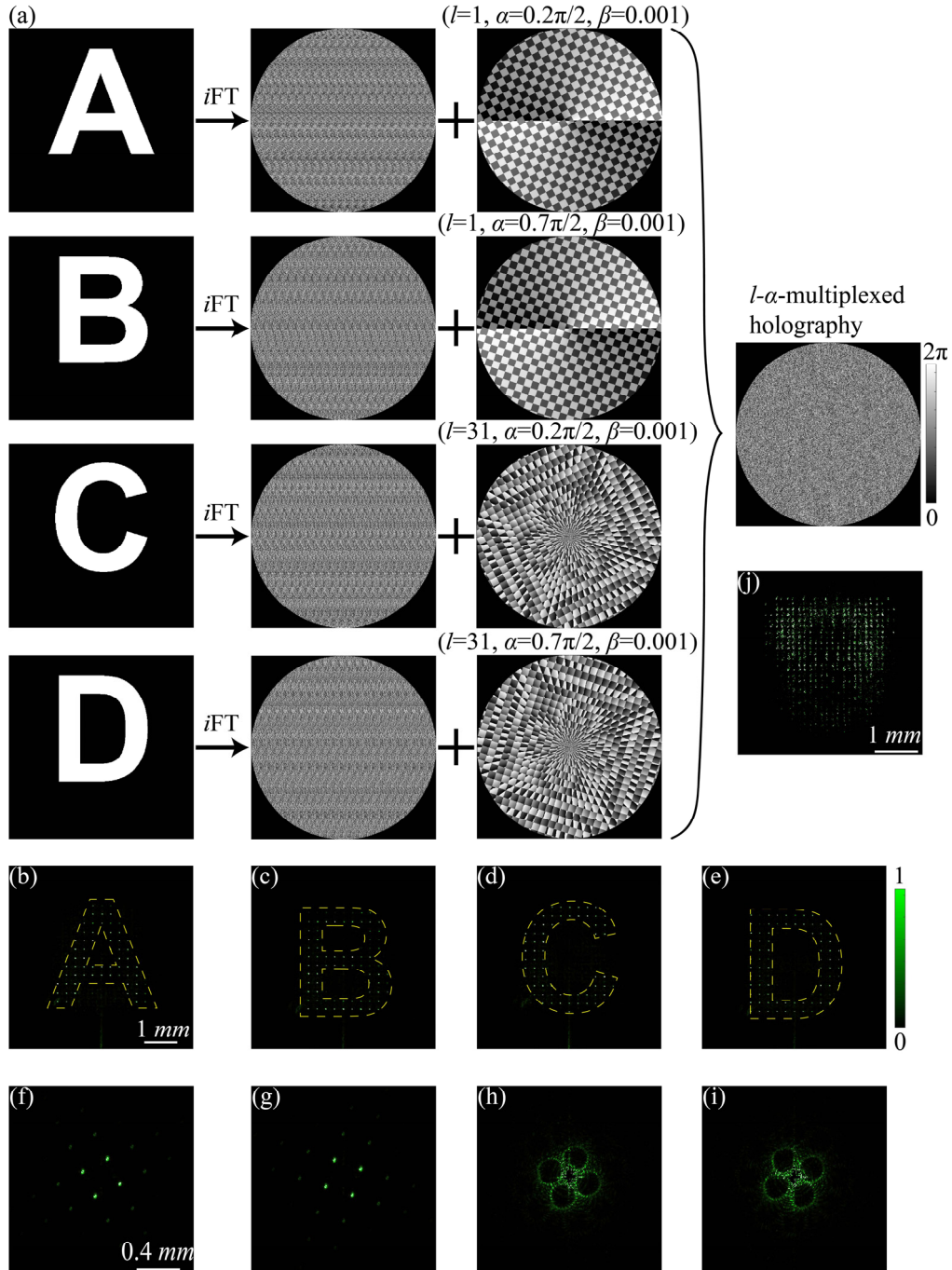

Fig. S3 Experimental reconstruction results of the l-α-encrypted OAML-multiplexed holography.

(a) The design process and (b)–(i) experimental reconstruction results. (f)-(i) Capture intensity

distributions of the above VL beams, respectively. (j) Experimental reconstruction results of the OAML-preserved holography.

Supplementary Note4: The *l*-*β*-encrypted OAML-multiplexed holography

The *l*-*β*-encrypted OAML-multiplexed holography is shown in Fig. S4. Two different topological charges (*l*=1 and 31) and two different constants *β* (*β*=0.001 and 0.004) are used to encode the four images with the letters "E", "F", "G" and "H". One *l*-*β*-encrypted OAML-multiplexed hologram can be obtained by superimposing the four OAM selective holograms generated from the OAM-preserved holograms and four OAML phase modes with (*l*=1, *α*=0.2*π*/2, *β*=0.001), (*l*=1, *α*=0.2*π*/2, *β*=0.004), (*l*=31, *α*=0.2*π*/2, *β*=0.001) and (*l*=31, *α*=0.2*π*/2, *β*=0.004). Here *l* and *β* together determine the encrypted and decrypted images. The four images can be reconstructed when the multiplexed hologram is illuminated by different OAML beams with (*l*=-1, {*α*}*=-0.2*π*/2, {*β*}*=-0.001), (*l*=-1, {*α*}*=-0.2*π*/2, {*β*}*=-0.004), (*l*=-31, {*α*}*=-0.2*π*/2, {*β*}*=-0.001) and (*l*=-31, {*α*}*=-0.2*π*/2, {*β*}*=-0.004), respectively, as shown in Figs. S4(b)–S4(e). Figures S4(f)-S4(i) illustrate the capture intensity distributions of the aforementioned VL beams, respectively. Upon illumination of the multiplexed OAML-preserved hologram by a planar beam, four images manifest simultaneously, appearing indistinguishable from each other, as depicted in Fig. S4(j).
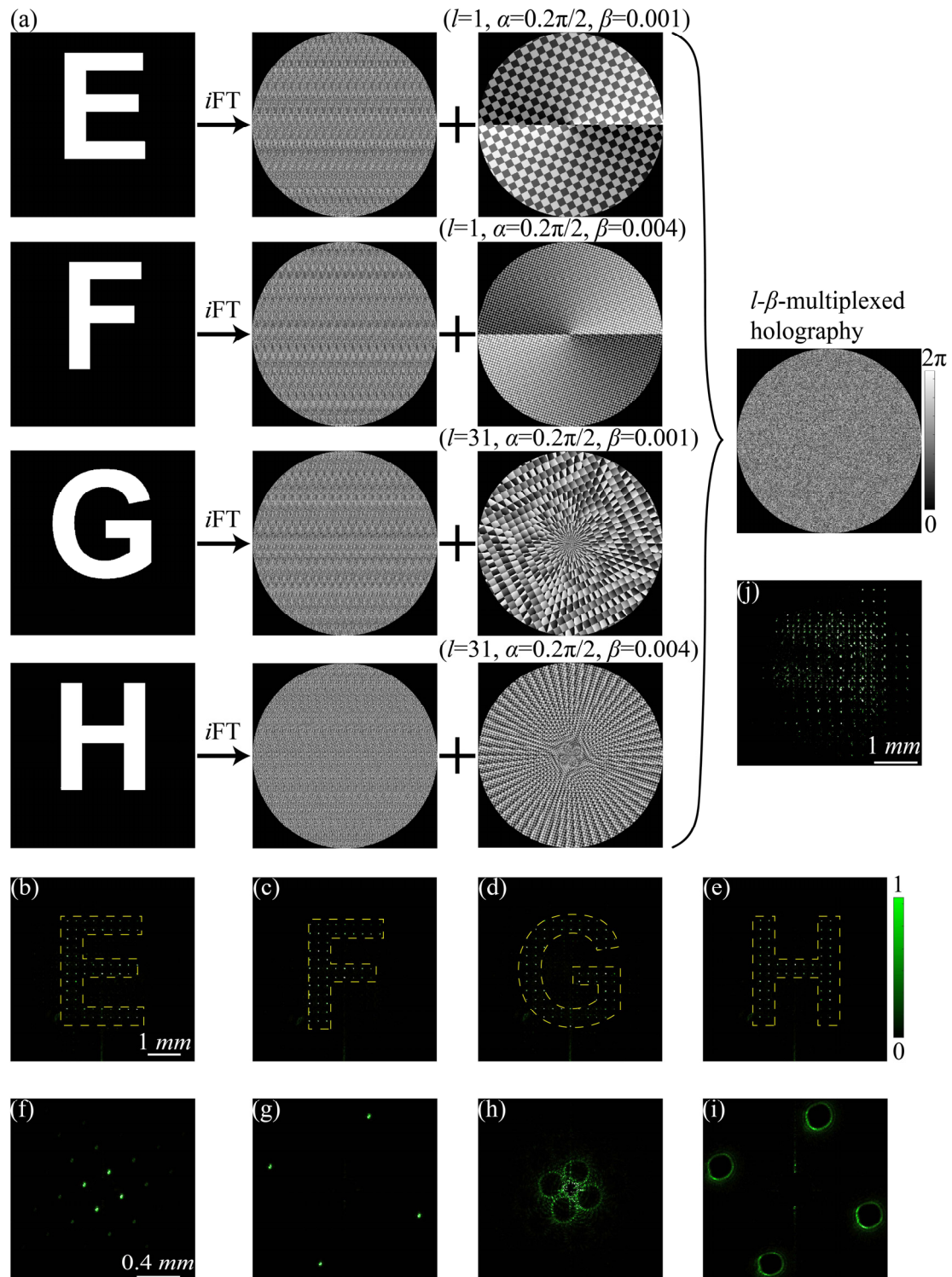
Fig. S4 Experimental reconstruction results of the *l-β*-encrypted OAML-multiplexed holography.

(a) The design process and (b)–(i) experimental reconstruction results. (f)-(i) Capture intensity

distributions of the above VL beams, respectively. (j) Experimental reconstruction results of the

OAML-preserved holography.

Supplementary Note5: The *α-β*-encrypted OAML-multiplexed holography

The α-β-encrypted OAML-multiplexed holography is shown in Fig. S5. Two different topological charges (α=0.2π/2 and 0.7π/2) and two different constants β (β=0.001 and 0.004) are used to encode the four images with the letters "E", "F", "G" and "H". One α-β-encrypted OAML-multiplexed hologram can be obtained by superimposing the four OAM selective holograms generated from the OAM-preserved holograms and four OAML phase modes with (l=1, α=0.2π/2, β=0.001), (l=1, α=0.2π/2, β=0.004), (l=1, α=0.7π/2, β=0.001) and (l=1, α=0.7π/2, β=0.004). Here α and β together determine the encrypted and decrypted images. The four images can be reconstructed when the multiplexed hologram is illuminated by different OAML beams with (l=-1, $\{\alpha\}$*=-0.2π/2, $\{\beta\}$*=-0.001), (l=-1, $\{\alpha\}$*=-0.2π/2, $\{\beta\}$*=-0.004), (l=-1, $\{\alpha\}$*=-0.7π/2, $\{\beta\}$*=-0.001) and (l=-1, $\{\alpha\}$*=-0.7π/2, $\{\beta\}$*=-0.004), respectively, as shown in Figs. S5(b)–S5(e). Figures S5(f)-S5(i) illustrate the capture intensity distributions of the aforementioned VL beams, respectively. Upon illumination of the multiplexed OAML-preserved hologram by a planar beam, four images manifest simultaneously, appearing indistinguishable from each other, as depicted in Fig. S5(j).
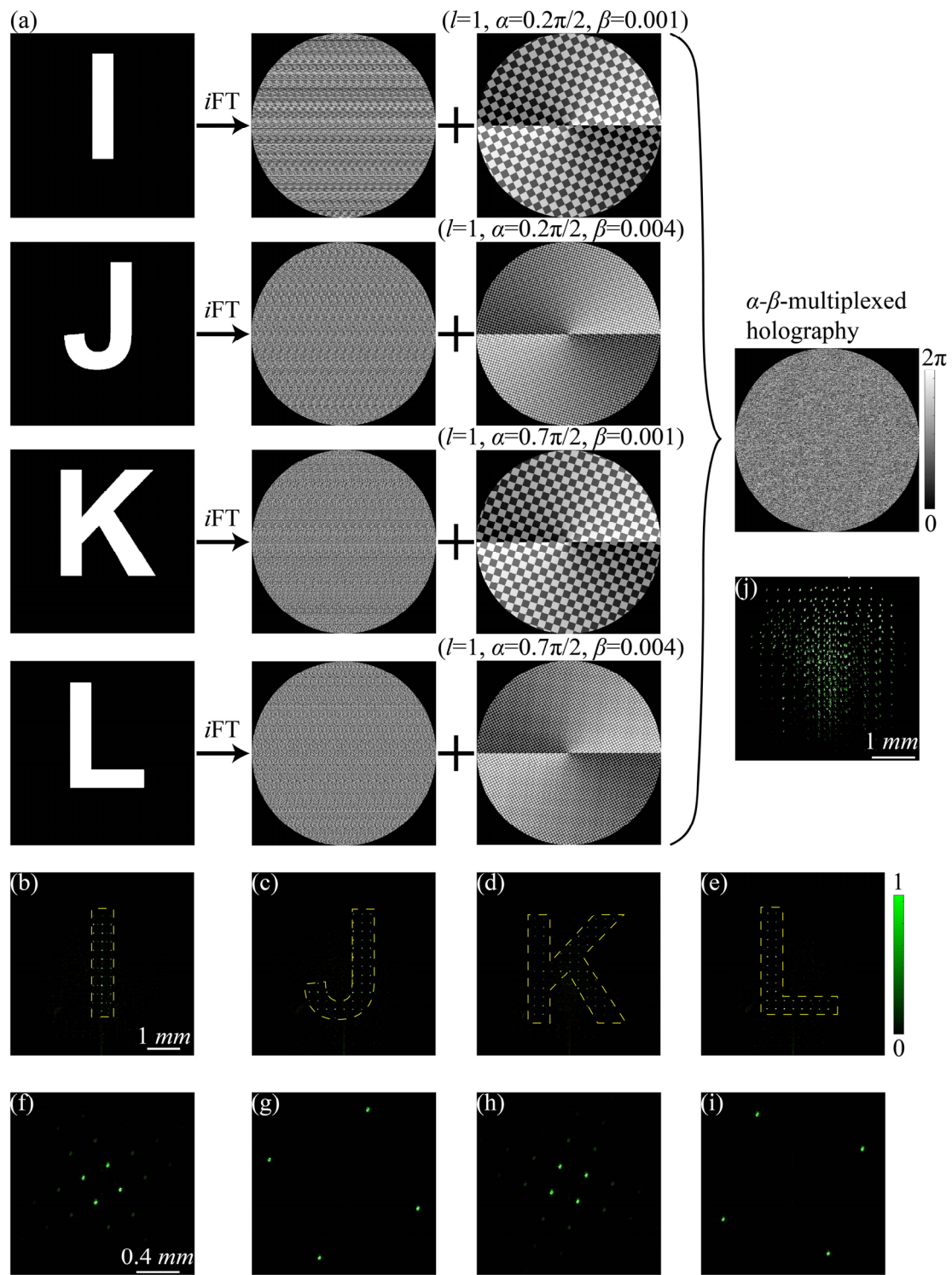
Fig. S5 Experimental reconstruction results of the α-β-encrypted OAML-multiplexed holography. (a) The design process and (b)–(i) experimental reconstruction results. (f)-(i) Capture intensity distributions of the above VL beams, respectively. (j) Experimental reconstruction results of the OAML-preserved holography.

Supplementary Note6: The l-α-β-encrypted OAML-multiplexed holography

The l-α-β-encrypted OAML-multiplexed holography is shown in Fig. S6. First, the principle of l-α-β-encrypted OAML-multiplexed holography is illustrated in Fig. S6(a). The eight images with "1A" to "1H" are encoded into eight holograms, then eight different OAML phase modes with (l=1, α=0.2π/2, β=0.001), (l=1, α=0.2π/2, β=0.004), (l=1, α=0.7π/2, β=0.001), (l=1, α=0.7π/2, β=0.004), (l=31, α=0.2π/2, β=0.001), (l=31, α=0.2π/2, β=0.004), (l=31, α=0.7π/2, β=0.001) and (l=31, α=0.7π/2, β=0.004) are added to the above eight holograms, resulting in the eight OAM selective holograms. The l-α-β-encrypted OAML-multiplexed hologram is obtained by superimposing all selective holograms. In the decryption process, the encrypted images can be reconstructed by the suitable incident OAML beams with (l=-1, $\{\alpha\}$*=-0.2π/2, $\{\beta\}$*=-0.001), (l=-1, $\{\alpha\}$*=-0.2π/2, $\{\beta\}$*=-0.004), (l=-1, $\{\alpha\}$*=-0.7π/2, $\{\beta\}$*=-0.001), (l=-1, $\{\alpha\}$*=-0.7π/2, $\{\beta\}$*=-0.004), (l=-31, $\{\alpha\}$*=-0.2π/2, $\{\beta\}$*=-0.001), (l=-31, $\{\alpha\}$*=-0.2π/2, $\{\beta\}$*=-0.004), (l=-31, $\{\alpha\}$*=-0.7π/2, $\{\beta\}$*=-0.001) and (l=-31, $\{\alpha\}$*=-0.7π/2, $\{\beta\}$*=-0.004), as shown in Fig. S6(b). Thus, the combination of these parameters provides a high level of information security. Figures S6(c) illustrate the capture intensity distributions of the aforementioned VL beams, respectively. Upon illumination of the multiplexed OAML-preserved hologram by a planar beam, four images manifest simultaneously, appearing indistinguishable from each other, as depicted in Fig. S6(d).
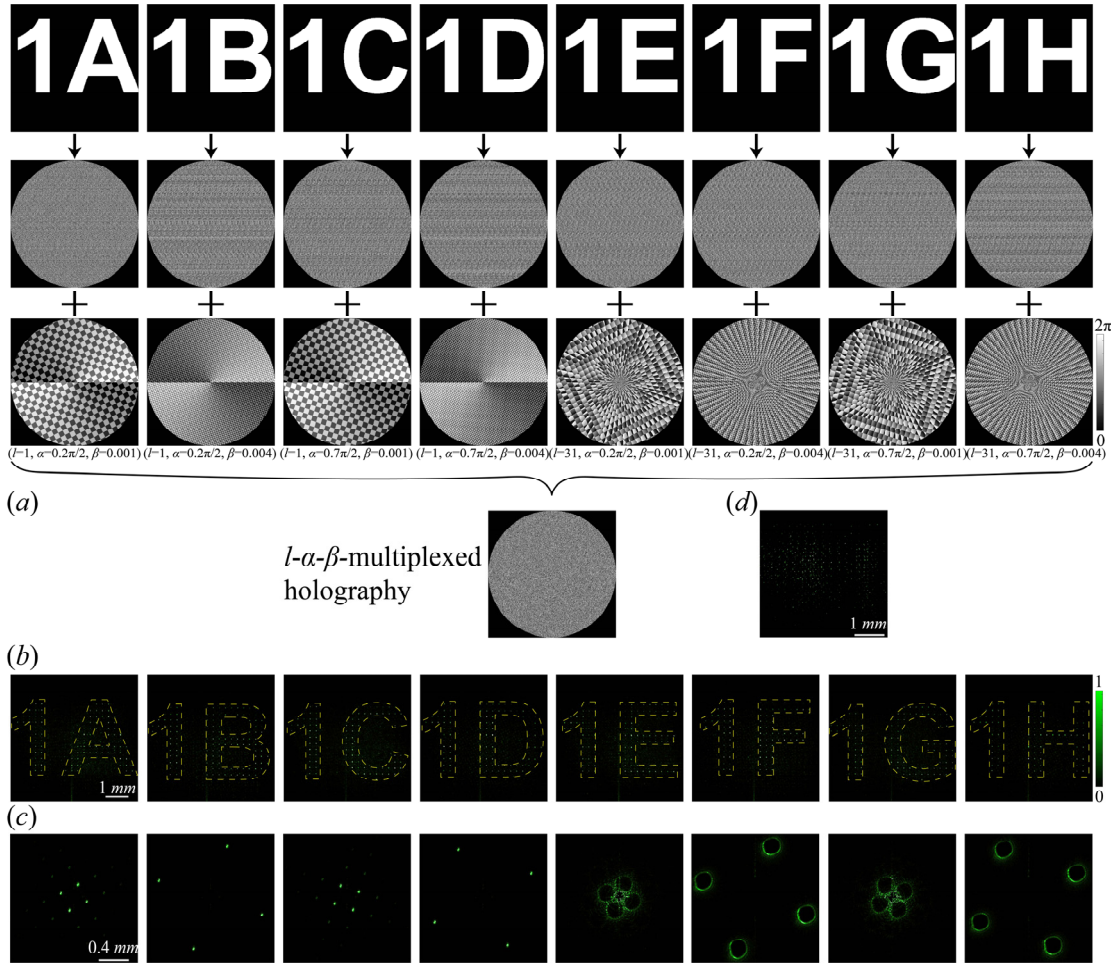
(*l*−1, *α*−0.2π/2, *β*−0.001) (*l*−1, *α*−0.2π/2, *β*−0.004) (*l*−1, *α*−0.7π/2, *β*−0.001) (*l*−1, *α*−0.7π/2, *β*−0.004)(*l*−31, *α*−0.2π/2, *β*−0.001)(*l*−31, *α*−0.2π/2, *β*−0.004)(*l*−31, *α*−0.7π/2, *β*−0.001)(*l*−31, *α*−0.7π/2, *β*−0.004)

(*a*)

l-α-β-multiplexed holography

(*d*)

(*b*)

(*c*)

Fig. S6 Experimental reconstruction results of the *l-α-β*-encrypted OAML-multiplexed holography. (a) Design process and (b) experimental reconstruction results. (c) Capture intensity distributions of the above VL beams, respectively. (d) Experimental reconstruction results of the OAML-preserved holography.